Letter

Ice-rule driven vertex frustration in a stretched pentagonal spin ice

Davis Crater,[1] Anya C. Lätti,[2] Michael Saccone,[3] Kevin Hofhuis,[4] Duncan Miertschin,[1] Balaram Regmi,[1] Barat Achinuq,[5] Armin Kleibert,[4] Charlotte F. Petersen,[2] and Alan Farhan[1,*]

[1]*Department of Physics, Baylor University, One Bear Place, Waco, Texas 76798, USA*

[2]*School of Chemistry, University of Melbourne, Melbourne, Victoria 3010, Australia*

[3]*Center for Nonlinear Studies and Theoretical Division, Los Alamos National Laboratory, Los Alamos, New Mexico 87545, USA*

[4]*Paul Scherrer Institut, Forschungsstrasse 111, 5232 Villigen PSI, Switzerland*

[5]*Lawrence Berkeley National Laboratory, One Cyclotron Road, Berkeley, California 94720, USA*

(Received 20 June 2024; accepted 20 November 2024; published 16 December 2024)

We introduce the stretched pentagonal spin ice and study low-energy configurations achieved after thermal annealing. Using synchrotron-based photoemission electron microscopy, we reveal highly disordered configurations dominated by short-range order. Real-space observations reveal that an adherence to local order, in the form of a strict ice-rule obedience, acts as a main factor in enforcing vertex frustration and hindering long-range order. Our results open up pathways to create forms of frustrated systems that have seemed elusive thus far.

DOI: 10.1103/PhysRevResearch.6.L042064

Artificial spin-ice systems, comprising single-domain nanomagnets lithographically defined onto two- and three-dimensional geometries, allow for the direct visualization of various frustration-driven phenomena by means of real-space magnetic microscopy [1]. Examples range from direct observations of a Coulomb phase with associated emergent magnetic monopoles and their dynamics [2–5], phase transitions [6–8], spin-glass behavior [9], and magnonic crystals [10–12] to emergent phenomena appearing in vertex-frustrated artificial spin ices [13–17]. These vertex-frustrated systems, be they the shakti-, tetris-, Santa Fe-, or Apamea lattice, are exclusively based on decimated square ices. All these artificial spin-ice systems exhibit four- and three-nanomagnet vertices combined into arrangements that hinder long-range ground-state ordering. The differences in activation energies for three- and four-nanomagnet vertices seem to play a main role in the emergence of vertex frustration [16] and associated emergent phenomena. The presence of four-nanomagnet vertices remained a crucial ingredient in all vertex-frustrated systems. Despite a variety of artificial spin ices built from three-nanomagnet vertices such as the artificial Kagome spin ice [6,7,18], triangular- [19], tripod- [20], or brickwork artificial spin ice [21], none of them features properties associated with vertex frustration. In fact, the emergence of vertex frustration in geometries dominated by three-nanomagnet vertices seemed impossible, so far. Here, we overcome this obstacle by introducing the stretched pentagonal spin ice (see Fig. 1) to the family of artificial spin-ice systems.

The main building block of the stretched pentagonal spin ice are colinear pairs of nanomagnets (lengths $L = 300$ nm and widths $W = 100$ nm) with a constant center-to-center distance $a = 400$ nm [see Fig. 1(a)]. One end of these pairs is arranged to meet at kagome-type three-nanomagnet vertices, defined by a variable lattice parameter b, and connect the kagome vertices with T-shaped three-nanomagnet vertices. The distance between vertices is constant, and lattice parameter c, defining the T-shaped vertices, consequently varies with b. This results in the formation of stretched pentagons interlinked via kagome- and T-shaped vertices [see Fig. 1(a)]. The consequence of such a dipolar tiling is a lattice dominated by three-nanomagnet vertices, void of any four-nanomagnet vertices. On one hand, highly frustrated kagome vertices with equal competing nearest-neighbor interactions result in sixfold degenerate ice-rule obeying moment configurations [19,22–24] [see purple frame in Fig. 1(b)]. On the other hand, in the T-shaped vertices, ice-rule obeying states are energetically split into type A ground-state configurations and higher-energy type B vertices [see yellow frame in Fig. 1(b)]. The latter are also known as *unhappy vertices* [25]. In the created stretched pentagonal lattice, these two forms of three-nanomagnet vertices are connected either directly with each other or via two-nanomagnet vertices [see Fig. 1(a)], where moment configurations are energetically listed as type α and type β vertices [see blue frame in Fig. 1(b)].

To experimentally realize this stretched pentagonal spin ice, a 2.6-nm-thick permalloy (Ni-80% Fe-20%) thin film was patterned using electron beam lithography. The choice of lateral dimensions and thickness of the patterned nanomagnets ensures access to thermally driven moment reorientations above 160 K [17,26]. Following sample fabrication, the sample was kept in vacuum at 300 K for over 20 days before it was transferred to cryogenic x-ray photoemission electron microscopy (X-PEEM) [27], an annealing procedure successfully employed in other artificial spin-ice systems [3,15,17].

*Contact author: alan_farhan@baylor.edu

Published by the American Physical Society under the terms of the Creative Commons Attribution 4.0 International license. Further distribution of this work must maintain attribution to the author(s) and the published article's title, journal citation, and DOI.

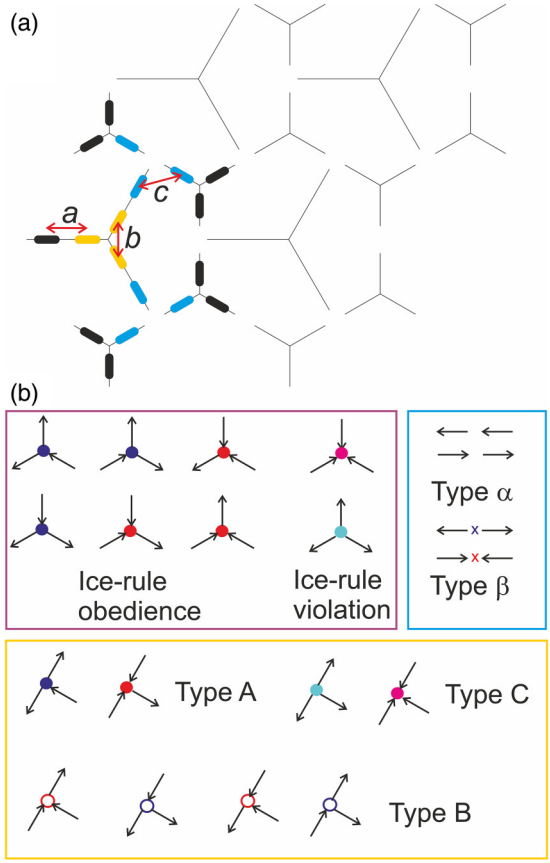


FIG. 1. (a) The stretched pentagonal spin ice consisting of Ising-type nanomagnets with lengths $L = 300$ nm and widths $W = 100$ nm placed on a background lattice resulting in colinear pairs of nanomagnets (center-to-center distance a), which connect kagome vertices (distance parameter b) with T-shaped three-nanomagnet vertices (distance parameter c). Internanomagnet interactions are varied by varying parameters b and c, while maintaining a as constant. (b) Possible vertex types listed with increasing dipolar energy. At kagome vertices (purple frame) there are six energetically degenerate ice-rule configurations and two ice-rule violating configurations. At two-nanomagnet vertices (blue frame) type α corresponds to head-to-tail moment alignments, while type β corresponds to head-to-head or tail-to-tail moment alignments. At T-shaped vertices (yellow frame), ice-rule obeying states are split into type A ground states and type B higher-energy configurations. Type C corresponds to ice-rule violations.

Magnetic imaging was performed taking advantage of x-ray magnetic circular dichroism (XMCD) at the Fe L3 edge [28]. Images with circular right $c+$ and circular left $c-$ polarized x-rays are recorded. Then, an XMCD image results from a pixel-wise division of these images ($c+/c-$). The obtained XMCD contrast is a measure of the projection of the magnetization on the x-ray polarization vector, so that nanomagnets with a magnetization parallel to the x-ray polarization appear black and those antiparallel to it appear white. Considering an x-ray incidental angle of 30° with respect to the sample surface, X-PEEM is primarily sensitive to in-plane magnetization components. After the weeks-long annealing period at 300 K, the sample was cooled to 110 K and magnetic images of low-energy configurations were recorded [see Figs. 2(a)–2(c)].

A look at these moment configurations reveals an interesting picture. For all investigated lattice spacings, $b = 346$, 433, and 520 nm, no clear visual features of long-range order are observed [see Figs. 2(a)–2(c)], as no obvious periodicially repeated ordering patterns over a length scale of several lattice parameters can be visually identified. This is further confirmed when analyzing these low-energy states in terms of vertex populations. At the three-nanomagnet vertices, be they T-shaped or kagome vertices, we see a very strong obedience to the local ice rules [see Figs. 2(d) and 2(e)], while the two-nanomagnet vertices also feature a dominant preference for type α vertices. Beyond obeying these local low-energy constraints, the systems lack signatures of long-range ordering. Furthermore, we observe a staggering presence of *unhappy* type B vertices, which reach an almost equal population around 50% for all investigated lattice parameters.

A comparison of these experimental observations with expected populations derived from kinetic Monte Carlo (KMC) simulations [26,29–31] (see Supplemental Material for more detailed information [32]) reveals a good agreement overall. However, one crucial difference is observed: the KMC-simulated configurations do feature up to 9%−10% ice-rule violations, while experimentally accessed low-energy states remain within a stricter ice-rule regime with violations remaining below 5%. An interesting observation from this comparison is that the increase in ice-rule violations at the kagome vertices in simulated configurations coincides with an increase in type A ground-state vertices at the T-shaped vertex sites. It provides a first hint that the enhanced presence of type B vertices is a direct consequence of ice-rule obedience at the kagome sites. One interesting feature from both experimental and simulated observations is that they both feature a crossing point, where type A and type B vertex populations become fully equalized [see Fig. 2(d)], hinting toward a lattice parameter b that potentially features the highest degree of vertex frustration.

While vertex populations provide statistical analysis on preferred local ordering preferences, they do not yield full information on global ordering preferences, if any. To do so, we performed an analysis on spatial correlation measures, for both magnetic moments and emergent magnetic charges residing at the vertices [13,17] (see Fig. 3). To determine the correlation C of a given magnetic moment with neighboring magnetic moments as a function of distance, we consider the dipolar interactions between spins falling within an increasing radius. Pairs of magnetic moments with directions that minimize dipolar interactions are assigned a correlation measure of -1, while those that maximize dipolar interaction will be assigned a correlation value of $+1$. The results are then averaged for all nanomagnets within a given field of view and all repeated annealed structures. Then, the average results with associated standard deviations are plotted as a function of distance R normalized against the double lattice parameter $2a$ [see Fig. 3(a)]. The same is then done, regarding the spatial charge-charge correlation measures C_q, taking a Coulomb-type interaction between emergent magnetic charges at the vertices [see Fig. 1(b)] into account [33,34]. Charge pairs that minimize their Coulomb interaction are assigned a correlation $C_q = -1$, while pairs that maximize their interaction are assigned $C_q = +1$. The results are then calculated and averaged

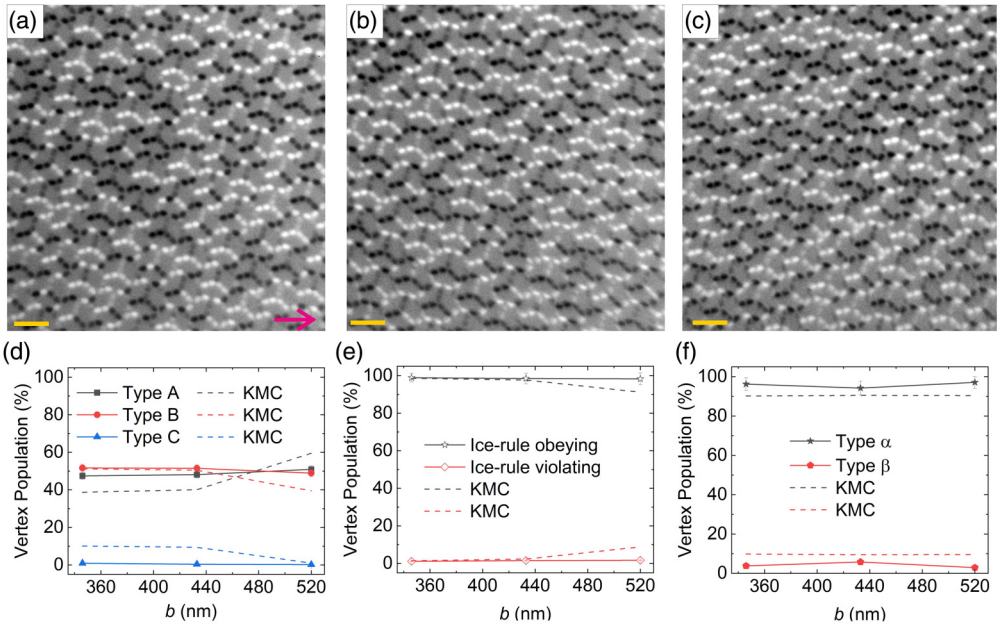


FIG. 2. (a)–(c) XMCD images of low-energy states achieved in stretched pentagonal spin-ice structures with lattice parameters (a) $b = 346$ nm, (b) $b = 433$ nm, and (c) $b = 520$ nm, after thermal annealing. The red arrow indicates the direction of incoming x-rays. The XMCD contrast is a measure of magnetic moment orientations with respect to incoming x-rays. Moments pointing toward the x-rays appear dark, while moments opposing the incoming x-ray direction will appear bright. The yellow scale bars represent a length of 2 μm. (d)–(f) Vertex-type population achieved after thermal annealing at (d) T-shaped vertices, (e) kagome vertices, and (f) two-nanomagnet vertices. The error bars stand for standard deviations from averaging over up to ten annealed configurations for each lattice parameter b. In (d)–(f) the dashed lines represent vertex populations extracted from kinetic Monte Carlo simulations.

as a function of distance for all recorded images. Looking at the spatial spin-spin correlation measure as a function of distance [see Fig. 3(a)], we see a clear dominance of short-range order manifested by nearest-neighbor ($R/2a$) moments exhibiting average correlation measures around -0.4, while correlation measures beyond the nearest neighbors quickly diminish toward 0. When looking at the spatial charge-charge correlation measures we see a result comparable to artificial kagome spin ice [35] with correlations rapidly diminishing, with only nearest-neighbor charges appearing to exhibit a detectable nonvanishing correlation measure, while anything beyond nearest-neighbor charges appears to be randomly ordered [see Fig. 3(b)]. Exploring spatial moment correlations in the form of magnetic structure factors [2,3,19] was also undertaken [32]. There, experimentally achieved low-energy states are compared with simulated patterns that strictly adhere to ice rules at the kagome vertices, but are otherwise fully randomized. We see strong similarities of these configurations with experimental observations (see Fig. 1 in Supplemental Material [32]), further strengthening conclusions on the short-range ordered nature of the stretched pentagonal artificial spin ice.

All results discussed so far show clear features of short-range order dominated by local ice-rule obedience and the absence of long-range order. Furthermore, the almost perfect 50/50 population of type A and type B vertices is a typical feature of vertex-frustrated systems [13,15,17]. In all vertex-frustrated artificial spin ices known, the vertex frustration emerges as a result of a complex interplay between four- and three-nanomagnet vertices. However, in the stretched pentagonal spin ice, the simultaneous strict adherence to ice-rule constraints, particularly at the kagome vertices, and vertex frustration suggests that both patterns must be interlinked with one another.

To confirm this suspicion we take a closer look at the imaged low-energy configurations and analyze kinetic pathways around the kagome vertices that would result in converting type B into type A vertices at the T-shaped vertices, and whether such kinetic pathways would constitute ice-rule violations or not. In Figs. 4(a) and 4(b) we see typical examples where we highlighted kagome vertices with surrounding moment configurations organized in such a way that involved type B vertices (highlighted with cyan blue dots) are forbidden to convert to type A, as such a conversion would constitute ice-rule violations at the highlighted kagome vertices [see orange dots in Figs. 4(a) and 4(b)]. These ice-rule enforced unhappy type B vertices are seen in significant numbers throughout all investigated lattice spacings. A statistical analysis of all annealed configurations as a function of lattice parameter b, we observe that over 30% of all kagome vertices consistently involve such forbidden relaxation pathways, featuring only a modest decay with increasing lattice spacing b [see Fig. 4(c)]. This decay further confirms that the stronger the nearest-neighbor coupling at kagome vertices is, the stronger an enhanced presence of type B vertices at T-shaped vertices will be. All together, these observations clearly reveal a strict obedience to local order in the form of ice rules at the kagome vertices and how it directly results in a lack of global long-range order, as a staggering presence of type B vertices is enforced at the T-shaped vertices.

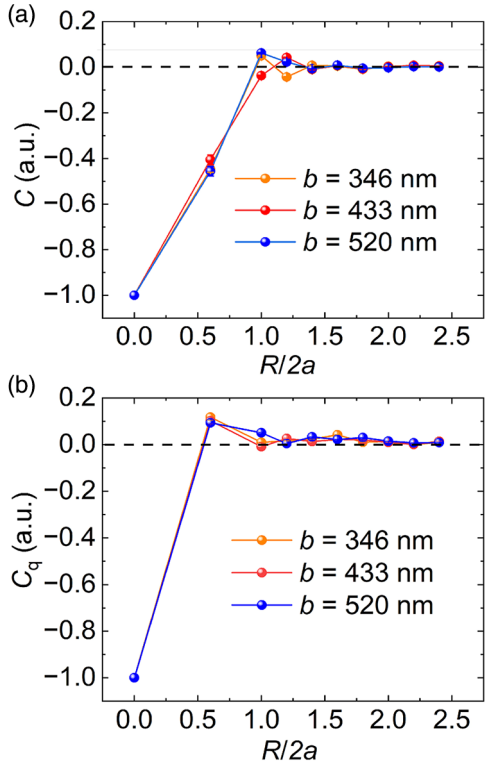


FIG. 3. (a) Average spatial spin-spin correlation measure plotted as a function of normalized distance. (b) Average charge-charge correlation measure plotted as a function of normalized distance. Error bars, which are in the same order of magnitude as the symbol sizes, represent standard deviations stemming from averaging over up to ten annealed configurations.

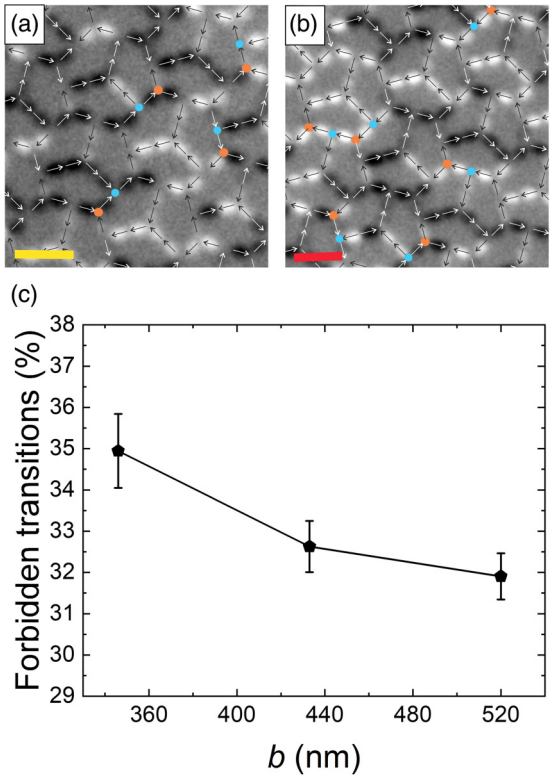


FIG. 4. (a) and (b) Cropped XMCD images of stretched pentagonal spin-ice arrays with lattice spacings $b = 346$ nm and $b = 433$ nm, respectively. Highlighted with orange dots are typical examples of kagome vertices, which in their strong ice-rule obedience prevent neighboring T-shaped vertices captured in a type B vertex state (blue dots) from converting into type A vertices. The yellow bar in (a) and red bar in (b) correspond to a length of 1 μm. (c) Percentages of kagome vertices that involve forbidden moment reversals, as a result of the strict ice-rule obedience, all plotted as a function of lattice spacing. The error bars stand for standard deviations resulting from analyzing over ten annealed stretched pentagonal structures for each lattice parameter.

In summary, the stretched pentagonal spin ice features an ice-rule driven vertex frustration and short-range correlations. The realization of vertex frustration systems dominated by three-nanomagnet vertices remained an elusive concept so far [13–15], demonstrating the power of creative lattice design to develop new branches within the tree of artificial spin-ice systems [1]. Furthermore, important open questions remain open regarding the stretched pentagonal spin ice, including that of the actual ground-state and temperature-dependent phase transitions, potentially addressed via simulations [33,34] and experiments [7,36].

This research used resources of the Advanced Light Source, which is a DOE Office of Science User Facility under Contract No. DE-AC02-05CH11231. Part of this work was performed at the SIM Beamline of the Swiss Light Source. C.F.P. was supported by the Selby Scientific Foundation through the Selby Research Award.

[1] S. H. Skjærvø, C. H. Marrows, R. L. Stamps, and L. J. Heyderman, Advances in artificial spin ice, Nat. Rev. Phys. **2**, 13 (2019).

[2] Y. Perrin, B. Canals, and N. Rougemaille, Extensive degeneracy, Coulomb phase and magnetic monopoles in artificial square ice, Nature (London) **540**, 410 (2016).

[3] A. Farhan, M. Saccone, C. F. Petersen, S. Dhuey, R. V. Chopdekar, Y.-L. Huang, N. Kent, Z. Chen, M. J. Alava, T. Lippert, A. Scholl, and S. van Dijken, Emergent magnetic monopole dynamics in macroscopically degenerate artificial spin ice, Sci. Adv. **5**, eaav6380 (2019).

[4] S. Ladak, D. E. Read, G. K. Perkins, L. F. Cohen, and W. R. Branford, Direct observation of magnetic monopole defects in an artificial spin-ice system, Nat. Phys. **6**, 359 (2010).

[5] E. Östman, H. Stopfel, I.-A. Chioar, U. B. Arnalds, A. Stein, V. Kapaklis, and B. Hjörvarsson, Interaction modifiers in artificial spin ices, Nat. Phys. **14**, 375 (2018).

[6] B. Canals, I.-A. Chioar, V.-D. Nguyen, M. Hehn, D. Lacour, F. Montaigne, A. Locatelli, T. O. Menteş, B. S. Burgos, and N. Rougemaille, Fragmentation of magnetism in artificial kagome dipolar spin ice, Nat. Commun. **7**, 11446 (2016).

[7] K. Hofhuis, S. H. Skjærvø, S. Parchenko, H. Arava, Z. Luo, A. Kleibert, P. M. Derlet, and L. J. Heyderman, Real-space imaging of phase transitions in bridged artificial kagome spin ice, Nat. Phys. **18**, 699 (2022).

[8] V. Schánilec, B. Canals, V. Uhlíř, L. Flajšman, J. Sadílek, T. Šikola, and N. Rougemaille, Bypassing dynamical freezing in artificial kagome ice, Phys. Rev. Lett. **125**, 057203 (2020).

[9] M. Saccone, F. Caravelli, K. Hofhuis, S. Parchenko, Y. A. Birkhölzer, S. Dhuey, A. Kleibert, S. van Dijken, C. Nisoli, and A. Farhan, Direct observation of a dynamical glass transition in a nanomagnetic artificial Hopfield network, Nat. Phys. **18**, 517 (2022).

[10] S. Gliga, E. Iacocca, and O. G. Heinonen, Dynamics of reconfigurable artificial spin ice: Toward magnonic functional materials, APL Mater. **8**, 040911 (2020).

[11] E. Iacocca, S. Gliga, and O. G. Heinonen, Tailoring spin-wave channels in a reconfigurable artificial spin ice, Phys. Rev. Appl. **13**, 044047 (2020).

[12] M. B. Jungfleisch, W. Zhang, E. Iacocca, J. Sklenar, J. Ding, W. Jiang, S. Zhang, J. E. Pearson, V. Novosad, J. B. Ketterson, O. Heinonen, and A. Hoffmann, Dynamic response of an artificial square spin ice, Phys. Rev. B **93**, 100401(R) (2016).

[13] I. Gilbert, G.-W. Chern, S. Zhang, L. O'Brien, B. Fore, C. Nisoli, and P. Schiffer, Emergent ice rule and magnetic charge screening from vertex frustration in artificial spin ice, Nat. Phys. **10**, 670 (2014).

[14] I. Gilbert, Y. Lao, I. Carrasquillo, L. O'Brien, J. D. Watts, M. Manno, C. Leighton, A. Scholl, C. Nisoli, and P. Schiffer, Emergent reduced dimensionality by vertex frustration in artificial spin ice, Nat. Phys. **12**, 162 (2016).

[15] M. Saccone, F. Caravelli, K. Hofhuis, S. Dhuey, A. Scholl, C. Nisoli, and A. Farhan, Real-space observation of ergodicity transitions in artificial spin ice, Nat. Commun. **14**, 5674 (2023).

[16] H. Stopfel, E. Östman, I.-A. Chioar, D. Greving, U. B. Arnalds, T. P. A. Hase, A. Stein, B. Hjörvarsson, and V. Kapaklis, Magnetic order and energy-scale hierarchy in artificial spin-ice structures, Phys. Rev. B **98**, 014435 (2018).

[17] M. Saccone, K. Hofhuis, Y.-L. Huang, S. Dhuey, Z. Chen, A. Scholl, R. V. Chopdekar, S. van Dijken, and A. Farhan, Dipolar cairo lattice: Geometrical frustration and short-range correlations, Phys. Rev. Mater. **3**, 104402 (2019).

[18] A. Farhan, P. M. Derlet, A. Kleibert, A. Balan, R. V. Chopdekar, M. Wyss, L. Anghinolfi, F. Nolting, and L. J. Heyderman, Exploring hyper-cubic energy landscapes in thermally active finite artificial spin-ice systems, Nat. Phys. **9**, 375 (2013).

[19] K. Hofhuis, C. F. Petersen, M. Saccone, S. Dhuey, A. Kleibert, S. van Dijken, and A. Farhan, Geometrical frustration and competing orders in the dipolar trimerized triangular lattice, Phys. Rev. B **104**, 014409 (2021).

[20] X. Zhang, I.-A. Chioar, G. Fitez, A. Hurben, M. Saccone, N. S. Bingham, J. Ramberger, C. Leighton, C. Nisoli, and P. Schiffer, Artificial magnetic tripod ice, Phys. Rev. Lett. **131**, 126701 (2023).

[21] J. Park, B. L. Le, J. Sklenar, G.-W. Chern, J. D. Watts, and P. Schiffer, Magnetic response of brickwork artificial spin ice, Phys. Rev. B **96**, 024436 (2017).

[22] A. S. Wills, R. Ballou, and C. Lacroix, Model of localized highly frustrated ferromagnetism: The kagomé spin ice, Phys. Rev. B **66**, 144407 (2002).

[23] Y. Qi, T. Brintlinger, and J. Cumings, Direct observation of the ice rule in an artificial kagome spin ice, Phys. Rev. B **77**, 094418 (2008).

[24] A. Farhan, P. M. Derlet, L. Anghinolfi, A. Kleibert, and L. J. Heyderman, Magnetic charge and moment dynamics in artificial kagome spin ice, Phys. Rev. B **96**, 064409 (2017).

[25] M. J. Morrison, T. R. Nelson, and C. Nisoli, Unhappy vertices in artificial spin ice: new degeneracies from vertex frustration, New J. Phys. **15**, 045009 (2013).

[26] A. Farhan, A. Scholl, C. F. Petersen, L. Anghinolfi, C. Wuth, S. Dhuey, R. V. Chopdekar, P. Mellado, M. J. Alava, and S. van Dijken, Thermodynamics of emergent magnetic charge screening in artificial spin ice, Nat. Commun. **7**, 12635 (2016).

[27] A. Doran, M. Church, T. Miller, G. Morrison, A. T. Young, and A. Scholl, Cryogenic PEEM at the advanced light source, J. Electron Spectrosc. Relat. Phenom. **185**, 340 (2012).

[28] J. Stöhr, Y. Wu, B. D. Hermsmeier, M. G. Samant, G. R. Harp, S. Koranda, D. Dunham, and B. P. Tonner, Element-specific magnetic microscopy with circularly polarized x-rays, Science **259**, 658 (1993).

[29] G. T. Barkema and M. E. J. Newman, Monte Carlo simulation of ice models, Phys. Rev. E **57**, 1155 (1998).

[30] A. Bortz, M. Kalos, and J. Lebowitz, A new algorithm for Monte Carlo simulation of Ising spin systems, J. Comput. Phys. **17**, 10 (1975).

[31] A. Farhan, C. F. Petersen, S. Dhuey, L. Anghinolfi, Q. H. Qin, M. Saccone, S. Velten, C. Wuth, S. Gliga, P. Mellado, M. J. Alava, A. Scholl, and S. van Dijken, Nanoscale control of competing interactions and geometrical frustration in a dipolar trident lattice, Nat. Commun. **8**, 995 (2017).

[32] See Supplemental Material at http://link.aps.org/supplemental/10.1103/PhysRevResearch.6.L042064 for details on utilized Kinetic Monte Carlo Methods and magnetic structure factor calculations can be found in this document.

[33] G. Möller and R. Moessner, Magnetic multipole analysis of kagome and artificial spin-ice dipolar arrays, Phys. Rev. B **80**, 140409(R) (2009).

[34] G.-W. Chern, P. Mellado, and O. Tchernyshyov, Two-stage ordering of spins in dipolar spin ice on the kagome lattice, Phys. Rev. Lett. **106**, 207202 (2011).

[35] S. Zhang, I. Gilbert, C. Nisoli, G.-W. Chern, M. J. Erickson, L. O'Brien, C. Leighton, P. E. Lammert, V. H. Crespi, and P. Schiffer, Crystallites of magnetic charges in artificial spin ice, Nature (London) **500**, 553 (2013).

[36] L. Anghinolfi, H. Luetkens, J. Perron, M. G. Flokstra, O. Sendetskyi, A. Suter, T. Prokscha, P. M. Derlet, S. L. Lee, and L. J. Heyderman, Thermodynamic phase transitions in a frustrated magnetic metamaterial, Nat. Commun. **6**, 8278 (2015).